Geophysical Research Letters

RESEARCH LETTER
10.1029/2018GL080122

Special Section:
Initial results of the ERG (Arase) project and multi-point observations in geospace

Longitudinal Structure of Oxygen Torus in the Inner Magnetosphere: Simultaneous Observations by Arase and Van Allen Probe A

M. Nosé[1], A. Matsuoka[2], A. Kumamoto[3], Y. Kasahara[4], J. Goldstein[5,6], M. Teramoto[1], F. Tsuchiya[3], S. Matsuda[2], M. Shoji[1], S. Imajo[1], S. Oimatsu[7], K. Yamamoto[7], Y. Obana[8], R. Nomura[9], A. Fujimoto[10], I. Shinohara[2], Y. Miyoshi[1], W. S. Kurth[11], C. A. Kletzing[11], C. W. Smith[12], and R. J. MacDowall[13]

[1]Institute for Space-Earth Environmental Research, Nagoya University, Nagoya, Japan, [2]Institute of Space and Astronautical Science, Japan Aerospace Exploration Agency, Sagamihara, Japan, [3]Graduate School of Science, Tohoku University, Sendai, Japan, [4]Graduate School of Natural Science and Technology, Kanazawa University, Kanazawa, Japan, [5]Space Science and Engineering Division, Southwest Research Institute, San Antonio, TX, USA, [6]Department of Physics and Astronomy, University of Texas at San Antonio, San Antonio, TX, USA, [7]Graduate School of Science, Kyoto University, Kyoto, Japan, [8]Faculty of Engineering, Osaka Electro-Communication University, Neyagawa, Japan, [9]Research of Interior Structure and Evolution of Solar System Bodies, National Astronomical Observatory of Japan, Tokyo, Japan, [10]Graduate School of Computer Science and Systems Engineering, Kyushu Institute of Technology, Iizuka, Japan, [11]Department of Physics and Astronomy, University of Iowa, Iowa City, IA, USA, [12]Institute for the Study of Earth, Oceans, and Space, University of New Hampshire, Durham, NH, USA, [13]Solar System Exploration Division, Goddard Space Flight Center, Greenbelt, MD, USA

Key Points:
- Simultaneous observations by Arase and Van Allen Probe A are used to examine the longitudinal structure of an oxygen torus
- Only Arase detected an enhancement of the average plasma mass up to ~3.5 amu around L = 4.9-5.2 and MLT = 5.0 hr
- For this event, the longitudinal extent of the O^+ density enhancement is better described as a crescent-shaped torus or a pinched torus

Correspondence to:
M. Nosé,
nose.masahito@isee.nagoya-u.ac.jp

Citation:
Nosé, M., Matsuoka, A., Kumamoto, A., Kasahara, Y., Goldstein, J., Teramoto, M., et al. (2018). Longitudinal structure of oxygen torus in the inner magnetosphere: Simultaneous observations by Arase and Van Allen Probe A. *Geophysical Research Letters*, *45*, 10,177–10,184. https://doi.org/10.1029/2018GL080122

Received 20 AUG 2018
Accepted 26 SEP 2018
Accepted article online 1 OCT 2018
Published online 10 OCT 2018

Abstract Simultaneous observations of the magnetic field and plasma waves made by the Arase and Van Allen Probe A satellites at different magnetic local time (MLT) enable us to deduce the longitudinal structure of an oxygen torus for the first time. During 04:00–07:10 UT on 24 April 2017, Arase flew from L = 6.2 to 2.0 in the morning sector and detected an enhancement of the average plasma mass up to ~3.5 amu around L = 4.9–5.2 and MLT = 5.0 hr, implying that the plasma consists of approximately 15% O^+ ions. Probe A moved outbound from L = 2.0 to 6.2 in the afternoon sector during 04:10–07:30 UT and observed no clear enhancements in the average plasma mass. For this event, the O^+ density enhancement in the inner magnetosphere (i.e., oxygen torus) does not extend over all MLT but is skewed toward the dawn, being described more precisely as a crescent-shaped torus or a pinched torus.

Plain Language Summary In the early 1980s, it was discovered that the O^+ ion density is sometimes enhanced in a limited range of altitude in the deep inner magnetosphere (approximately 10,000-km to 30,000-km altitude). This O^+ density enhancement was originally named the *oxygen torus*, which implies azimuthal symmetry of the density enhancement. However, its longitudinal structure remains poorly known. This study investigates the longitudinal structure of the oxygen torus for the first time using simultaneous observations from the Arase and Van Allen Probe A satellites. We find that the oxygen torus does not extend over all longitudes but is localized to the dawn sector, indicating a crescent-shaped torus.

1. Introduction

Chappell (1982) examined data from the retarding ion mass spectrometer (RIMS) instrument carried by the Dynamic Explorer (DE) 1 satellite and discovered that the O^+ ion density is sometimes enhanced in a limited range of L shell in the deep inner magnetosphere. This O^+ density enhancement was originally called the *oxygen torus* by Chappell (1982) and Horwitz et al. (1984). Since then, some studies confirmed the oxygen torus around L = 3–5 during a storm recovery phase with a direct measurement by using the DE-1/RIMS data (Comfort et al., 1988; Horwitz et al., 1986; Roberts et al., 1987) and with an indirect measurement by combining observations of standing Alfvén waves (i.e., ULF waves) and plasma waves in the VLF/LF bands (Fraser et al., 2005; Grew et al., 2007; Maeda et al., 2009; Nosé et al., 2015, 2011; Obana et al., 2010; Takahashi et al., 2006, 2008).

Although the term oxygen torus implies azimuthal symmetry of the O^+ density enhancement, there has been only one statistical study about magnetic local time (MLT) distribution of the oxygen torus by Roberts et al. (1987) who found broad peaks of the occurrence distribution in the premidnight and morning sectors. No simultaneous observations of the oxygen torus at different MLT by multiple satellites have been

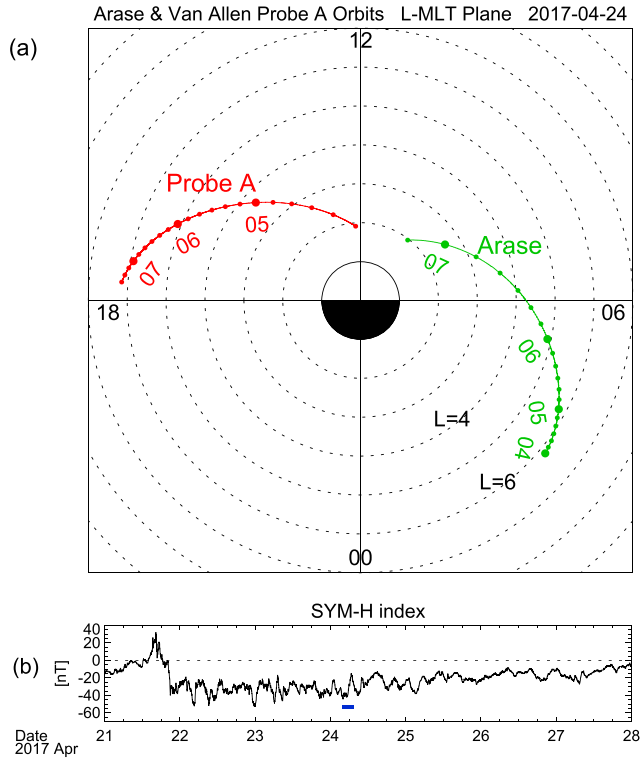

Figure 1. (a) Orbits of the Arase satellite during 04:00–07:10 UT and the Van Allen Probe A satellite during 04:10–07:30 UT on 24 April 2017 in the *L*-MLT plane. (b) The SYM-H index for 21–27 April 2017. A horizontal blue bar indicates the time interval of 04:00–07:30 UT on 24 April 2017 when the Arase and Probe A observations were made. MLT = magnetic local time.

performed. Now is a good time to investigate the MLT distribution of the oxygen torus, because two missions are currently making observations in the deep inner magnetosphere, at radial distances below 6.0 R_E, and at widely spaced MLT. The first is the Exploration of energization and Radiation in Geospace (ERG) *Arase* satellite (Miyoshi et al., 2018), and the second is the Van Allen Probes (Mauk et al., 2013). Both satellites carry instruments to measure magnetic field and plasma waves. From the resonant frequencies of standing Alfvén waves and the upper hybrid resonance (UHR) band, we can estimate the plasma mass density (ρ) and the electron number density (n_e), respectively. The average ion mass (M) is calculated by $M = (\rho - n_e m_e)/n_i \sim \rho/n_i \sim \rho/n_e$ under the assumption of quasi-neutrality of the plasma, where m_e is the electron mass and n_i is the ion number density.

This study reports simultaneous observations of M when both the Arase satellite and the Van Allen Probe A satellite traversed L = 2.0–6.2 around 04–08 UT on 24 April 2017. Arase was flying from predawn to morning, while Probe A moved from noon to dusk. We will examine if M was increased in a limited range of L on the dawn and/or dusk sides and reveal the longitudinal structure of oxygen torus for the first time on the basis of the simultaneous measurements at different longitudes.

2. Simultaneous Observations by Arase and Van Allen Probe A

2.1. Satellite Orbits and Geomagnetic Conditions

Figure 1a shows the orbital segments of Arase and Van Allen Probe A during the interval of interest. During 04:00–07:10 UT on 24 April 2017, Arase was flying along an inbound path from (L, MLT) = (6.2, 3.4 hr) to (2.0, 9.5 hr). Probe A was outbound from (L, MLT) = (2.0, 12.3 hr) to (6.2, 17.7 hr) at the almost same interval from 04:10 to 07:30 UT. Figure 1b displays the SYM-H index (Iyemori et al., 1992) for 21–27 April 2017. A horizontal blue bar indicates the time interval of 04:00–07:30 UT on 24 April 2017 when the Arase and Probe A observations were made. We found that a magnetic storm started around 18 UT on 21 April, and disturbances continued for approximately 2 days, followed by a gradual recovery from 24 to 27 April. This storm is considered to be a CIR (Corotating Interaction Regions) storm. The simultaneous observations were made when the strong disturbances ceased and the storm started to recover.

2.2. ULF Waves and UHR Waves

Figures 2a–2d compile the Arase observations during 04:00–07:10 UT on 24 April 2017. The top three panels are the dynamic power spectra of the magnetic field variations in the frequency range of 0–50 mHz in local magnetic (LMG) coordinates. The magnetic field data are obtained by Magnetic Field Experiment (MGF) (Matsuoka et al., 2018) and averaged over the spin period (~8 s). In LMG coordinates, the local magnetic field is defined by the combination of the International Geomagnetic Reference Field (IGRF)-12 internal model (Thébault et al., 2015) and the Tsyganenko, 1989 (T89) external model with Kp = 0 (Tsyganenko, 1989). The bottom panel shows the plasma wave spectrogram for the electric field in the frequency range of 5–600 kHz measured by the onboard frequency analyzer (OFA) and the high-frequency analyzer (HFA) of the Plasma Wave Experiment (PWE) (Kasahara et al., 2018; Kumamoto et al., 2018; Matsuda et al., 2018). In this spectrogram, data below and above 20 kHz come from OFA and HFA, respectively, resulting in appearance of a subtle change in the background emission level at 20 kHz. A white line delineates the local cyclotron frequency of electrons (f_{ce}) calculated from the MGF data.

No clear ULF wave signatures are identified in the radial and compressional components (Figures 2a and 2c), while there is a standing wave signature in the azimuthal component (Figure 2b); that is, the wave frequency becomes higher as the Arase satellite moves closer to the Earth. Strong wave power running until 06:40 UT at ~39 and ~49 mHz is due to artificial noises, which will be removed in future calibration. It is noteworthy that

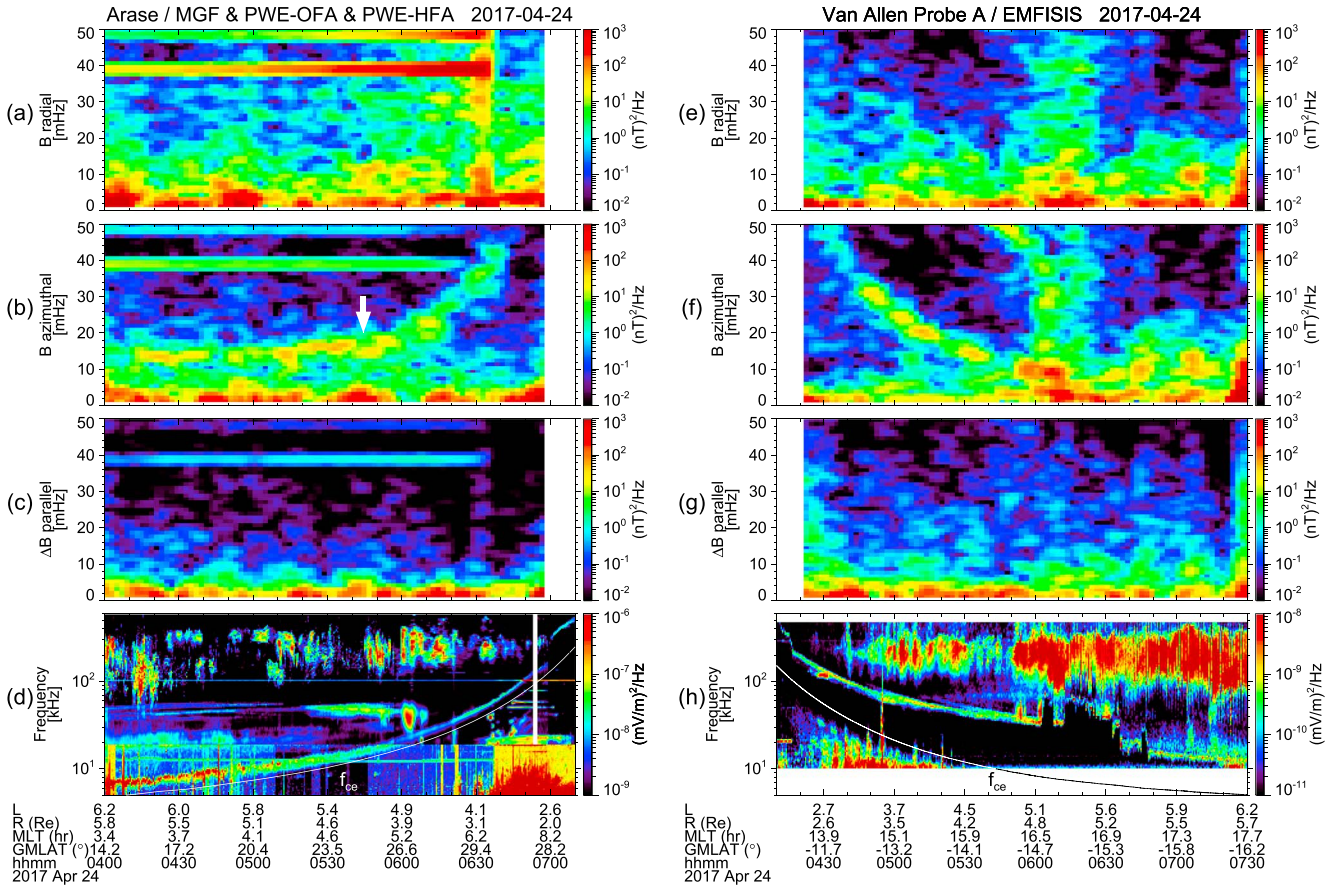

Figure 2. (a–d) Arase observations during 04:00–07:10 UT on 24 April 2017. The top three panels are the dynamic power spectra of the magnetic field variations in the radial, azimuthal, and compressional components measured by MGF. A white arrow indicates a time interval when toroidal wave frequency temporarily dropped. The bottom panel shows the plasma wave spectrogram for the electric field measured by PWE-OFA (<20 kHz) and PWE-HFA (≥20 kHz). A white line delineates the local cyclotron frequency of electrons. (e–h) Probe A observations during 04:10–07:30 UT on 24 April 2017. The format is the same as Figures 2a–2d except that data are obtained by EMFISIS. PWE = Plasma Wave Experiment; OFA = Onboard Frequency Analyzer; HFA = High-Frequency Analyzer; EMFISIS = Electric and Magnetic Field Instrument Suite and Integrated Science; MLT = magnetic local time; MGF = Magnetic Field Experiment.

the wave frequency does not monotonically increase but temporary drops at 05:40–05:50 UT as indicated by a white arrow. This implies that heavy ions are loaded, and the average plasma mass is increased, resulting in decreases of the Alfvén velocity and the standing wave frequency. In Figure 2d, we found clear emissions of UHR waves increasing gradually from <10 to ~150 kHz during 04:00–07:00 UT and showing a sudden jump to ~300 kHz around 07:00 UT. The jump in frequency of the UHR (f_{UHR}) is due to an enhancement of n_e.

Figures 2e–2h show the dynamic power spectra of the magnetic field variations and the plasma wave spectrogram of the electric field oscillation for Probe A. The format is the same as Figures 2a–2d except that the time interval is 04:10–07:30 UT and the plasma wave spectrogram covers the frequency range of 10–500 kHz. These data were measured by the Electric and Magnetic Field Instrument Suite and Integrated Science (EMFISIS) instrumentation suite (Kletzing et al., 2013). We found the standing wave signature in the azimuthal component (Figure 2f) of the magnetic field which is similar to that observed by Arase. Since Probe A was in an outbound pass, the wave frequency gradually decreases. In the radial and compressional components (Figures 2e and 2g), we recognize no standing wave signatures. In Figure 2h, UHR waves can be seen. Their frequency dropped at 04:15 UT, decreased smoothly during 04:15–06:00 UT, and showed irregular changes during 06:00–06:50 UT.

2.3. Mass Density, Electron Density, and Average Plasma Mass

From the dynamic power spectra of Figures 2b and 2f, we selected peak frequencies of the toroidal waves (f_T) to infer ρ. Selection criteria are similar to those used by Nosé et al. (2011, 2015). The selected frequencies are

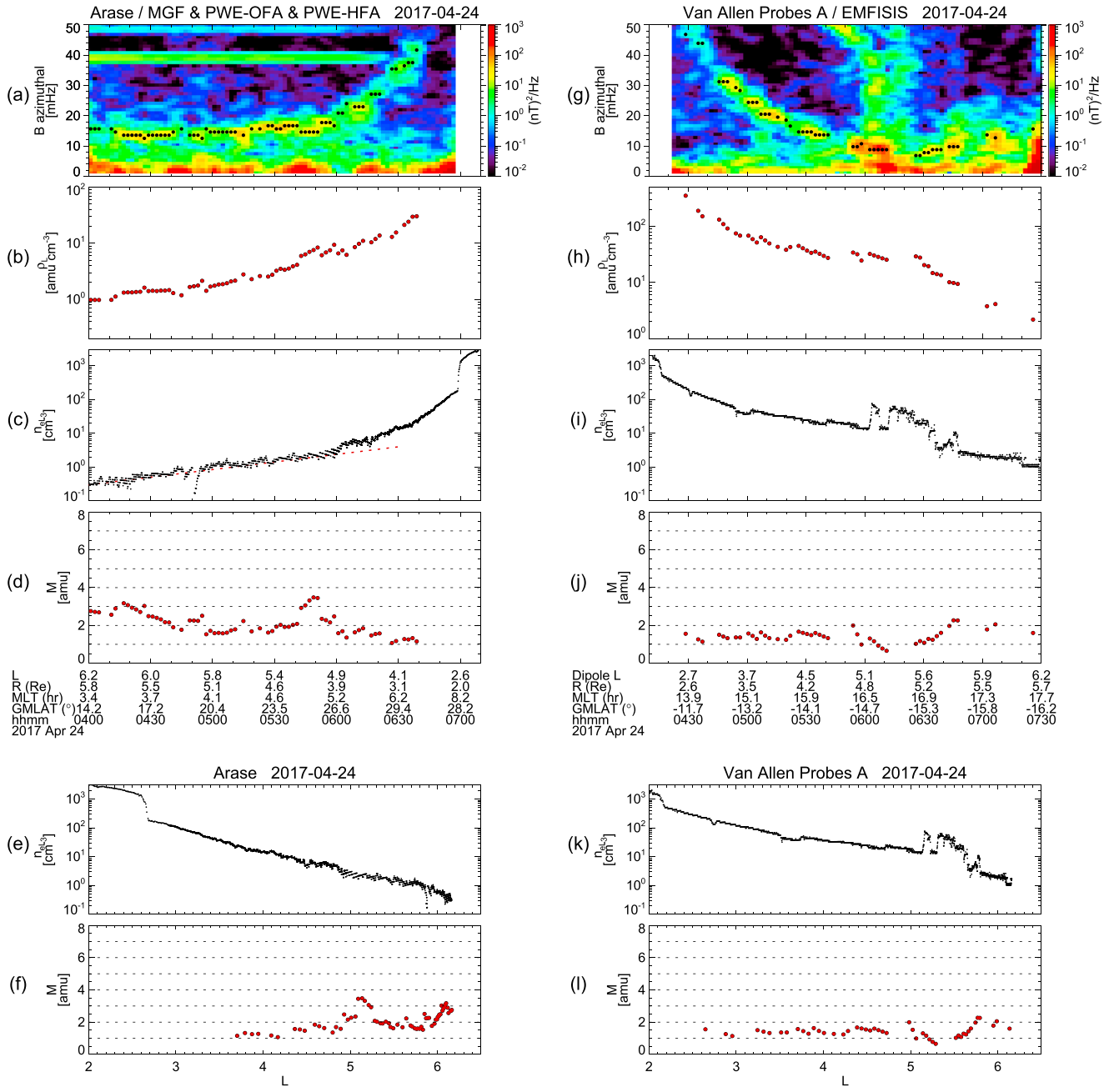

Figure 3. Arase observations of (a) the dynamic power spectrum of the magnetic field variations in the azimuthal component with selected peak frequency, (b) mass density, (c) electron density, and (d) average plasma mass, during 04:00–07:10 UT on 24 April 2017. (e and f) Electron density and average plasma mass as a function of *L*. (g–l) Same as in Figures 3a–3f but for the Probe A observations during 04:10–07:30 UT on 24 April 2017. PWE = Plasma Wave Experiment; OFA = Onboard Frequency Analyzer; HFA = High-Frequency Analyzer; EMFISIS = Electric and Magnetic Field Instrument Suite and Integrated Science; MLT = magnetic local time; MGF = Magnetic Field Experiment.

plotted with black circles over the dynamic power spectrum as shown in Figures 3a for Arase and Figure 3g for Probe A. Since these toroidal waves were clearly observed off the equatorial plane (absolute values of geomagnetic latitude ~10°–30°), they are considered to be fundamental mode waves. The magnetohydrodynamic wave equation in an arbitrary magnetic field geometry, which was introduced by Singer et al. (1981), was numerically solved to estimate ρ from f_T. The numerical calculation was made with the IGRF-12 and T89 (Kp = 4) magnetic field models and the power law model of the field-aligned

distribution of ρ (the power law index of 0.5); more details are given by Nosé et al. (2011, 2015). The estimation of ρ at satellite positions (ρ_L) is shown in Figure 3b for Arase and Figure 3h for Probe A.

We estimated the electron density at satellite positions (n_{eL}) from f_{UHR} and f_{ce} that appears in Figures 2d and 2h, using the equation $n_{eL} = 4\pi^2\varepsilon_0 m_e(f_{UHR}{}^2 - f_{ce}{}^2)/e^2$, where e is the electron charge and ε_0 is the vacuum permittivity. Results are shown in Figure 3c for Arase and Figure 3i for Probe A. The Arase satellite flying in the dawn flank found a steep inner gradient at 07:00 UT at (L, MLT) ~ (2.6, 8.2 hr). This is considered to be a recently eroded plasmapause. However, it should be noted that there is another change in the gradient of n_{eL} around 06:00 UT at (L, MLT) ~ (4.9, 5.2 hr); that is, as highlighted by a red dotted line, n_{eL} shows an upward shift after ~06:00 UT. Value of n_{eL} is less than a few cm^{-3} at 04:00–06:00 UT, while it is 5–200 cm^{-3} at 06:00–07:00 UT. These observations can be interpreted that the plasmatrough was at $L > 4.9$, and a partial refilling of plasma after erosion was taking place in the region at L = 2.6–4.9 (between the plasmapause and the plasmatrough). In the dusk flank, Probe A observed a possible plasmapause following an erosion event at 04:15 UT at (L, MLT) ~ (2.2, 13.0 hr). There are small temporal enhancements in n_{eL} during 06:00–06:50 UT, which can be considered to be the narrowing plume that appears often in the afternoon sector during storm recovery (e.g., Goldstein et al., 2004; Grebowsky, 1970). Between the plasmapause and the plume, n_{eL} was gradually falling but stayed at a rather large value of 20–500 cm^{-3}. This may reflect that the region was partially refilled. After 0650 UT, n_{eL} became a few cm^{-3}, indicating that Probe A was located in the plasmatrough.

Using the values of ρ_L and n_{eL}, we finally calculated M (~ρ_L/n_{eL}) as displayed in Figure 2d for Arase and Figure 2j for Probe A. It is found from Figure 2d that M was enhanced to 3.0–3.5 amu at 05:40–06:00 UT in a limited range of L (i.e., L = 4.9–5.2) at dawn (MLT ~ 5.0 hr). M was about 1–2 amu in the surrounding time periods, although it became as high as 2.5–3 amu at 04:00–04:30 UT. On the other hand, from the results in the afternoon sector (Figure 3j), no clear enhancements in M appeared. M stays generally at about 1–2 amu.

To investigate a relation between the variations of M and the structures of the plasma density, n_{eL} and M are plotted as a function of L in Figures 3e and 3f for Arase and in Figures 3k and 3l for Probe A. At dawn, we found the plasmapause at L ~ 2.6, the partially refilling region between L = 2.6 and 4.9, and the plasmatrough at $L > 4.9$ (Figure 3e). The enhancement of M up to 3.5 amu was located around L ~ 5.1 and just outside the plasmaspheric refilling region (Figure 3f). In the afternoon, however, there are the plasmapause at L ~ 2.1, the partially refilling region between L = 2.1 and 5.1, the plume at L = 5.1–5.8, and the plasmatrough at $L > 5.8$ (Figure 3k). M was 1–2 amu throughout L = 2.5–6.2 (Figure 3l).

3. Discussion

3.1. Interpretation of Enhancement of *M*

Although M is a parameter representing a degree of concentration of heavy ions (i.e., He^+, He^{++}, and O^+), it does not give information about their composition. If we assume that the observed enhancement of M up to 3.5 amu is created only by He^+, the plasma should consist of 17% H^+ and 83% He^+. Such plasma has an unrealistic composition of $n(He^+)/n(H^+)$ ~ 5, where n(A) is the number density of ion species A, because previous studies (Comfort et al., 1988; Horwitz et al., 1984) reported that $n(He^+)/n(H^+)$ at $L < 6$ is in the range of 0.01–1.0 and its typical value is 0.2–0.5.

Therefore, we need to consider the existence of O^+ ions. When we assume that a plasma consists of H^+, He^+, and O^+ ions as well as $n(He^+) = n(O^+)$, a plasma of 72% H^+, 14% He^+, and 14% O^+ has M ~ 3.5 amu and $n(He^+)/n(H^+)$ ~ 0.19. When a two-component plasma (i.e., H^+ and O^+) is considered, we find 83% H^+ and 17% O^+ to yield M ~ 3.5 amu. It is concluded that the plasma included ~15% of O^+ ions, and the Arase satellite detected the so-called oxygen torus around (L, MLT) ~ (5.1, 5.0 hr).

3.2. Generation Mechanism of Oxygen Torus and Its Longitudinal Structure

Previous studies (Comfort et al., 1988; Horwitz et al., 1986, 1990; Roberts et al., 1987) have proposed that ionospheric O^+ ions are extracted and supplied into a limited range of L in the inner magnetosphere to form the oxygen torus. This generation mechanism is as follows: the plasmasphere expands during the storm recovery phase; an interaction occurs between the ring current energetic ions and the plasmaspheric cold electrons in the limited L range; the plasmaspheric electrons are energized and precipitated into the underlying

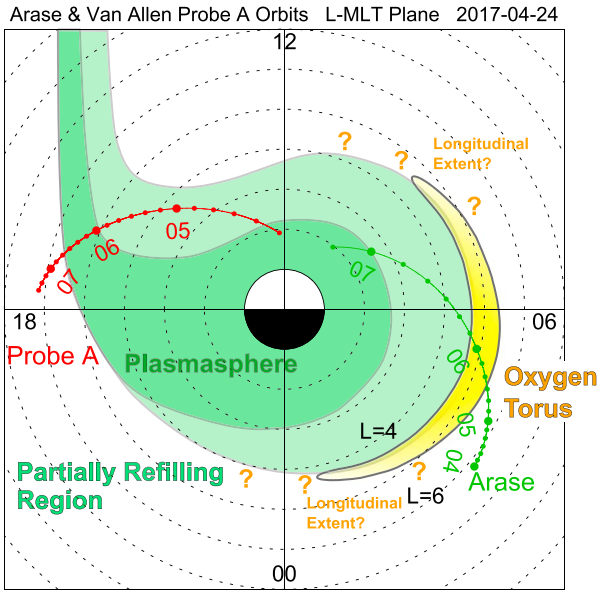

Figure 4. A schematic figure of the structures of the plasmasphere and the oxygen torus at 04:00–07:30 UT on 24 April 2017 inferred from the analysis results of the Arase and Probe A data as well as the generation scenario suggested by previous studies. MLT = magnetic local time.

ionosphere; it increases the ionospheric temperature and the scale height of ionospheric plasma, and then a large number of O^+ ions are extracted into the high altitude. With this mechanism we expect that an oxygen torus is formed in all MLT or preferentially near dusk, because during the storm recovery phase, the ring current becomes more axis-symmetric and the plasmasphere usually has a bulge at dusk. This is inconsistent with the present observational results (Figures 3f and 3l).

In another generation scenario proposed by Roberts et al. (1987), ionospheric O^+ ions are extracted from the dayside polar cusp during the initial or main phase of magnetic storms and transported into the near-Earth magnetosphere on the nightside. Then the plasmapause expands during the storm recovery phase and some parts of the ionospheric O^+ ions in the magnetosphere are trapped within the plasmasphere, resulting in formation of the oxygen torus. Recently, Nosé et al. (2015) performed numerical calculation of thermal O^+ ion trajectories in the inner magnetosphere during the storm recovery phase and revealed that O^+ ions are not only trapped within the plasmasphere but also draped around the plasmapause on the dawn and morning sides. The longitudinal structure of an oxygen torus expected from this mechanism is consistent with Figures 3f and 3l.

3.3. Longitudinal Structure of Oxygen Torus for the 24 April 2017 Event

Based on the analysis results of the Arase and Probe A data as well as the generation scenario suggested by previous studies (Nosé et al., 2015; Roberts et al., 1987), we draw in Figure 4 a schematic figure of the structures of the plasmasphere and the oxygen torus at 0400–0730 UT on 24 April 2017. The observations were made during the early phase of the storm recovery which was preceded by a long-lasting (~2 days) storm main phase (Figure 1b). Geomagnetic disturbances caused an erosion of the plasmasphere and a drainage plasma plume on the dayside. Because of the long-lasting main phase, the plasmasphere may shrink down to $L \sim 2.5$. The drainage plasma plume became narrow in longitude and moved to eastward in the afternoon during the following recovery phase (e.g., Goldstein et al., 2004; Grebowsky, 1970). This plasmaspheric structure is represented as a dark green region in Figure 4.

During the recovery phase, the convection electric field becomes weak and the open/closed separatrix for cold plasma (i.e., the boundary between a sunward convecting region and a corotating region) is expanded outward. Then the expanded closed region starts to be refilled with plasma of ionospheric origin and/or corotating plasmaspheric plasma. Partially refilling regions during the recovery phase are found by the IMAGE extreme ultraviolet (EUV) imager (Goldsten & Sandel, 2005). In Figure 4, such region is displayed with light green.

The oxygen torus is shown with a yellow region. It was found only by Arase in the dawn and just outside the partially refilling region. The present observations suggested that the oxygen torus does not extend over all MLT for the 24 April 2017 event. Its longitudinal structure would not be described by a torus but a crescent-shaped torus or a pinched torus, although its longitudinal extent is still unrevealed. Exploring this issue is left for future studies that employ multiple (more than three) satellites carrying magnetic field and plasma wave instruments or a satellite equipped with an EUV camera to image a global distribution of O^+ ions (Goldstein et al., 2018).

3.4. Other Issues About Structure of Oxygen Torus

It is worth briefly mentioning here the latitudinal extension of the oxygen torus. In the present study, we assume that M is constant at an L shell, which indicates that the oxygen torus uniformly extends along the geomagnetic field line. However, this may not be true in the actual inner magnetosphere. From the CRRES and IMAGE satellite data, Takahashi et al. (2004) and Denton et al. (2004, 2006) concluded that heavy ions are preferentially concentrated near the magnetic equator.

We should consider that the longitudinal extension of the oxygen torus would be temporally variable. In the time intervals before/after 04:00–07:30 UT on 24 April 2017, the oxygen torus may happen to be more axisymmetric (i.e., really torus shaped).

Thus, the latitudinal structure and temporal variation of the oxygen torus are also important issues to be examined in future studies. An EUV camera to capture the glow from O^+ ions will provide a global distribution of the oxygen torus and its temporal variations, if it is carried by satellites orbiting the Earth at 8–20 R_E (Goldstein et al., 2018). Such satellite mission will help solve these issues.

4. Conclusions

We examined the longitudinal structure of the oxygen torus for the first time, based on the simultaneous observations of the magnetic field and the plasma wave made by the Arase and Van Allen Probe A satellites at different MLT around 04:00–07:00 UT on 24 April 2017. Arase was flying along an inbound path from (L, MLT) = (6.2, 3.4 hr) to (2.0, 9.5 hr) during 04:00–07:10 UT, and Probe A was outbound from (L, MLT) = (2.0, 12.3 hr) to (6.2, 17.7 hr) at the almost same interval from 04:10 to 07:30 UT. Both satellites observed clear toroidal mode ULF oscillations and UHR waves. From their frequencies (f_T and f_{UHR}), we respectively estimated ρ_L and n_{eL} and consequently calculated M under the assumption of quasi-neutrality of plasma (i.e., $M \sim \rho_L/n_{eL}$).

Arase found an enhancement of M up to ~3.5 amu in a limited range of L (i.e., L = 4.9–5.2) at dawn (MLT ~ 5.0 hr), while M was about 1–2 amu in the neighboring region. This enhancement of M implies that the plasma includes approximately 15% of O^+ ions around L = 5 at dawn, suggesting an oxygen torus. From the results in the afternoon sector by Probe A, however, M showed no clear enhancements and stayed generally at about 1–2 amu. These observational results led us to make a sketch of the plasmasphere and the oxygen torus as shown in Figure 4. It seems that for the 24 April 2017 event the oxygen torus does not extend over all MLT but is skewed toward the dawn, being described more precisely as a crescent-shaped torus or a pinched torus.

Acknowledgments
Science data of the ERG (Arase) satellite were obtained from the ERG Science Center operated by ISAS/JAXA and ISEE/Nagoya University (https://ergsc.isee.nagoya-u.ac.jp/index.shtml.en). The Arase satellite data will be publicly available via ERG Science Center on a project-agreed schedule. The present study analyzed the MGF L2_v01.01 data, the PWE-OFA L2_v02_01 data, and the PWE-HFA L2_v01_01 data. The Van Allen Probes/EMFISIS data are available at http://emfisis.physics.uiowa.edu. The present study used the EMFISIS L3_v1.6.1 data. The electron number density data at Probe A position were obtained on request to W. S. Kurth and provided with L4_v1.5.15. The SYM-H index is provided by the World Data Center for Geomagnetism, Kyoto, and is available at http://wdc.kugi.kyoto-u.ac.jp. Geomagnetic field by the IGRF-12 and T89 models is calculated with GEOPACK routines developed by N. A. Tsyganenko and coded by H. Korth. This study is supported by the Japan Society for the Promotion of Science (JSPS), Grant-in-Aid for Scientific Research (B) (grant 16H04057), Challenging Research (Pioneering) (grant 17K18804), and Grant-in-Aid for Specially Promoted Research (grant 16H06286). Y. M. is supported by the Japan Society for the Promotion of Science (JSPS), Grant-in-Aid for Scientific Research on Innovative Areas (grant 15H05815). The work at the University of Iowa was performed through JHU/APL contract 921647 under NASA Prime contract NAS5-01072.

References

Chappell, C. R. (1982). Initial observations of thermal plasma composition and energetics from Dynamics Explorer-1. *Geophysical Research Letters*, *9*(9), 929–932. https://doi.org/10.1029/GL009i009p00929

Comfort, R. H., Newberry, I. T., & Chappell, C. R. (1988). Preliminary statistical survey of plasmaspheric ion properties from observations by DE 1/RIMS. In T. E. Moore, & J. H. Waite, Jr. (Eds.), *Modeling magnetospheric plasma*, *Geophysical Monograph Series* (Vol. 44, pp. 107–114). Washington, DC: American Geophysical Union. https://doi.org/10.1029/GM044p0107

Denton, R. E., Takahashi, K., Anderson, R. R., & Wuest, M. P. (2004). Magnetospheric toroidal Alfvén wave harmonics and the field line distribution of mass density. *Journal of Geophysical Research*, *109*, A06202. https://doi.org/10.1029/2003JA010201

Denton, R. E., Takahashi, K., Galkin, I. A., Nsumei, P. A., Huang, X., Reinisch, B. W., et al. (2006). Distribution of density along magnetospheric field lines. *Journal of Geophysical Research*, *111*, A04213. https://doi.org/10.1029/2005JA011414

Fraser, B. J., Horwitz, J. L., Slavin, J. A., Dent, Z. C., & Mann, I. R. (2005). Heavy ion mass loading of the geomagnetic field near the plasmapause and ULF wave implications. *Geophysical Research Letters*, *32*, L04102. https://doi.org/10.1029/2004GL021315

Goldstein, J., Chappell, C. R., Davis, M. W., Denton, M. H., Denton, R. E., Gallagher, D. L., et al. (2018). Imaging the global distribution of plasmaspheric oxygen. *Journal of Geophysical Research: Space Physics*, *123*, 2078–2103. https://doi.org/10.1002/2017JA024531

Goldstein, J., Sandel, B. R., Thomsen, M. F., Spasojević, M., & Reiff, P. H. (2004). Simultaneous remote sensing and in situ observations of plasmaspheric drainage plumes. *Journal of Geophysical Research*, *109*, A03202. https://doi.org/10.1029/2003JA010281

Goldsten, J., & Sandel, B. R. (2005). The global pattern of evolution of plasmaspheric drainage plumes. In J. Burch, M. Schulz, & H. Spence (Eds.), *Inner magnetosphere interactions: New perspectives from imaging*, *Geophysical Monograph Series* (Vol. 159, pp. 1–22). Washington, DC: American Geophysical Union. https://doi.org/10.1029/159GM02

Grebowsky, J. M. (1970). Model study of plasmapause motion. *Journal of Geophysical Research*, *75*(22), 4329–4333. https://doi.org/10.1029/JA075i022p04329

Grew, R. S., Menk, F. W., Clilverd, M. A., & Sandel, B. R. (2007). Mass and electron densities in the inner magnetosphere during a prolonged disturbed interval. *Geophysical Research Letters*, *34*, L02108. https://doi.org/10.1029/2006GL028254

Horwitz, J. L., Comfort, R. H., Brace, L. H., & Chappell, C. R. (1986). Dual-spacecraft measurements of plasmasphere-ionosphere coupling. *Journal of Geophysical Research*, *91*(A10), 11,203–11,216. https://doi.org/10.1029/JA091iA10p11203

Horwitz, J. L., Comfort, R. H., & Chappell, C. R. (1984). Thermal ion composition measurements of the formation of the new outer plasmasphere and double plasmapause during storm recovery phase. *Geophysical Research Letters*, *11*(8), 701–704. https://doi.org/10.1029/GL011i008p00701

Horwitz, J. L., Comfort, R. H., Richards, P. G., Chandler, M. O., Chappell, C. R., Anderson, P., et al. (1990). Plasmasphere-ionosphere coupling 2: Ion composition measurements at plasmaspheric and ionospheric altitudes and comparison with modeling results. *Journal of Geophysical Research*, *95*(A6), 7949–7959. https://doi.org/10.1029/JA095iA06p07949

Iyemori, T., Araki, T., Kamei, T., & Takeda, M. (1992). Mid-latitude geomagnetic indices ASY and SYM (provisional), no. 1, 1989–1990. In *Data analysis center for geomagnetism and space magnetism*. Kyoto, Japan: Kyoto University.

Kasahara, Y., Kasaba, Y., Kojima, H., Yagitani, S., Ishisaka, K., Kumamoto, A., et al. (2018). The plasma wave experiment (PWE) on board the Arase (ERG) satellite. *Earth, Planets and Space*, *70*(1), 86. https://doi.org/10.1186/s40623-018-0842-4

Kletzing, C. A., Kurth, W. S., Acuna, M., MacDowall, R. J., Torbert, R. B., Averkamp, T., et al. (2013). The electric and magnetic field instrument suite and integrated science (EMFISIS) on RBSP. *Space Science Reviews*, *179*(1-4), 127–181. https://doi.org/10.1007/s11214-013-9993-6

Kumamoto, A., Tsuchiya, F., Kasahara, Y., Kasaba, Y., Kojima, H., Yagitani, S., et al. (2018). High frequency analyzer (HFA) of plasma wave experiment (PWE) onboard the Arase spacecraft. *Earth, Planets and Space*, *70*(1), 82. https://doi.org/10.1186/s40623-018-0854-0

Maeda, N., Takasaki, S., Kawano, H., Ohtani, S., Decreau, P., Trotignon, J., et al. (2009). Simultaneous observations of the plasma density on the same field line by the CPMN ground magnetometers and the Cluster satellites. *Advances in Space Research*, *43*(2), 265–272. https://doi.org/10.1016/j.asr.2008.04.016

Matsuda, S., Kasahara, Y., Kojima, H., Kasaba, Y., Yagitani, S., Ozaki, M., et al. (2018). Onboard software of plasma wave experiment aboard Arase: Instrument management and signal processing of waveform capture/onboard frequency analyzer. *Earth, Planets and Space*, *70*(1), 75. https://doi.org/10.1186/s40623-018-0838-0

Matsuoka, A., Teramoto, M., Nomura, R., Nosé, M., Fujimoto, A., Tanaka, Y., et al. (2018). The Arase (ERG) magnetic field investigation. *Earth, Planets and Space*, *70*(1), 43. https://doi.org/10.1186/s40623-018-0800-1

Mauk, B. H., Fox, N. J., Kanekal, S. G., Kessel, R. L., Sibeck, D. G., & Ukhorskiy, A. (2013). Science objectives and rationale for the Radiation Belt Storm Probes Mission. *Space Science Reviews*, *179*(1-4), 3–27. https://doi.org/10.1007/s11214-012-9908-y

Miyoshi, Y., Shinohara, I., Takashima, T., Asamura, K., Higashio, N., Mitani, T., et al. (2018). Geospace exploration project ERG. *Earth, Planets and Space*, *70*(1), 101. https://doi.org/10.1186/10.1186/s40623-018-0862-0

Nosé, M., Oimatsu, S., Keika, K., Kletzing, C. A., Kurth, W. S., De Pascuale, S., et al. (2015). Formation of the oxygen torus in the inner magnetosphere: Van Allen Probes observations. *Journal of Geophysical Research: Space Physics*, *120*, 1182–1196. https://doi.org/10.1002/2014JA020593

Nosé, M., Takahashi, K., Anderson, R. R., & Singer, H. J. (2011). Oxygen torus in the deep inner magnetosphere and its contribution to recurrent process of O^+-rich ring current formation. *Journal of Geophysical Research*, *116*, A10224. https://doi.org/10.1029/2011JA016651

Obana, Y., Menk, F. W., & Yoshikawa, I. (2010). Plasma refilling rates for L = 2.3–3.8 flux tubes. *Journal of Geophysical Research*, *115*, A03204. https://doi.org/10.1029/2009JA014191

Roberts, W. T. Jr., Horwitz, J. L., Comfort, R. H., Chappell, C. R., Waite, J. H. Jr., & Green, J. L. (1987). Heavy ion density enhancements in the outer plasmasphere. *Journal of Geophysical Research*, *92*(A12), 13,499–13,512. https://doi.org/10.1029/JA092iA12p13499

Singer, H. J., Southwood, D. J., Walker, R. J., & Kivelson, M. G. (1981). Alfvén wave resonances in a realistic magnetospheric magnetic field geometry. *Journal of Geophysical Research*, *86*(A6), 4589–4596. https://doi.org/10.1029/JA086iA06p04589

Takahashi, K., Denton, R. E., Anderson, R. R., & Hughes, W. J. (2004). Frequencies of standing Alfvén wave harmonics and their implication for plasma mass distribution along geomagnetic field lines: Statistical analysis of CRRES data. *Journal of Geophysical Research*, *109*, A08202. https://doi.org/10.1029/2003JA010345

Takahashi, K., Denton, R. E., Anderson, R. R., & Hughes, W. J. (2006). Mass density inferred from toroidal wave frequencies and its comparison to electron density. *Journal of Geophysical Research*, *111*, A01201. https://doi.org/10.1029/2005JA011286

Takahashi, K., Ohtani, S., Denton, R. E., Hughes, W. J., & Anderson, R. R. (2008). Ion composition in the plasma trough and plasma plume derived from a combined release and radiation effects satellite magnetoseismic study. *Journal of Geophysical Research*, *113*, A12203. https://doi.org/10.1029/2008JA013248

Thébault, E., Finlay, C. C., Beggan, C. D., Alken, P., Aubert, J., Barrois, O., et al. (2015). International geomagnetic reference field: The 12th generation. *Earth, Planets and Space*, *67*(1), 79. https://doi.org/10.1186/s40623-015-0228-9

Tsyganenko, N. A. (1989). A magnetospheric magnetic field model with a warped tail current sheet. *Planetary and Space Science*, *37*(1), 5–20. https://doi.org/10.1016/0032-0633(89)90066-4